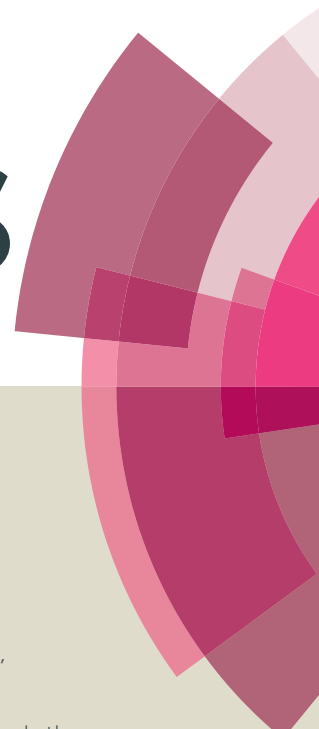


# RSC Advances



This article can be cited before page numbers have been issued, to do this please use: S. Fan, G. Chen, C. Li, C. Lv, Z. Han, J. Rao, Y. Hu and C. Zhang, *RSC Adv.*, 2015, DOI: 10.1039/C5RA19379F.



This is an *Accepted Manuscript*, which has been through the Royal Society of Chemistry peer review process and has been accepted for publication.

*Accepted Manuscripts* are published online shortly after acceptance, before technical editing, formatting and proof reading. Using this free service, authors can make their results available to the community, in citable form, before we publish the edited article. This *Accepted Manuscript* will be replaced by the edited, formatted and paginated article as soon as this is available.

You can find more information about *Accepted Manuscripts* in the [Information for Authors](#).

Please note that technical editing may introduce minor changes to the text and/or graphics, which may alter content. The journal's standard [Terms & Conditions](#) and the [Ethical guidelines](#) still apply. In no event shall the Royal Society of Chemistry be held responsible for any errors or omissions in this *Accepted Manuscript* or any consequences arising from the use of any information it contains.



## ARTICLE

## A novel visible-light-driven isocyanate silver photocatalyst: superior stability enhanced by intrinsic resonance effect

Shuo Fan,<sup>a</sup> Gang Chen,<sup>\*a</sup> Chunmei Li,<sup>a</sup> Chade Lv,<sup>a</sup> Zhonghui Han,<sup>a</sup> Jiancun Rao,<sup>b</sup> Yidong Hu<sup>a</sup> and Congmin Zhang<sup>a</sup>

Received 00th January 20xx,  
Accepted 00th January 20xx

DOI: 10.1039/x0xx00000x

www.rsc.org/

Isocyanate silver (AgNCO), a novel visible-light sensitive semiconductor photocatalyst is prepared based on an intrinsic resonance effect strategy through a simple precipitation process. The as-prepared photocatalyst exhibits photocatalytic degradation ability under visible light. Importantly, it also shows excellent photocatalytic stability which is a crucial problem of Ag-based photocatalyst to deal with. The existence of intrinsic resonance effect and crystal structure may be the main reasons for the superior photocatalytic stability of AgNCO photocatalyst. The possible transferred and separated behavior of charge carriers as well as the reason insight of outstanding photocatalytic stability are illustrated in detail. This work develops a new design idea for exploiting the stable Ag-based photocatalysts under visible light irradiation.

### Introduction

In recently years, semiconductor photocatalysts, as a kind of green solar energy conversion material, have drawn great attention because that they can employ in photodegrading organic contaminants and photocatalytic H<sub>2</sub> evolution from water efficiently under light irradiation.<sup>1–3</sup> Among them, Ag-based photocatalysts are regarded as a new family of promising photocatalytic materials because they exhibit high light utilization rate as well as unique decomposing organic pollutants and O<sub>2</sub> evolution ability from water splitting under solar light irradiation.<sup>4–7</sup> One of the significant reasons is that the hybridization of the energy band structure is related with participation from the filled d<sup>10</sup> electronic configuration of Ag<sup>+</sup> ion, which can facilitate the separation and transport of photogenerated electron-hole pairs, thus improving photocatalytic activity.<sup>8–11</sup> However, Ag-based photocatalytic materials are sensitive to light, so the photocorrosion can take place which leads to the poor photocatalytic stability and the decreasing of photocatalytic activity.<sup>12</sup> In order to overcome this obstacle, there are some attempts to inhibit the photocorrosion effect of Ag-based photocatalysts, such as importing electron acceptors or co-catalysts.<sup>13–15</sup> For example, Ag@AgVO<sub>3</sub>/rGO/PCN reported by Zhang and co-workers displays photodegradation activity and stability for organic dyes.<sup>16</sup> A novel series of β-AgAl<sub>1-x</sub>Ga<sub>x</sub>O<sub>2</sub> solid-solution photocatalysts synthesized by Ouyang and Ye shows the highest photocatalytic performance than β-AgAlO<sub>2</sub> and β-AgGaO<sub>2</sub>.<sup>17</sup> Nevertheless, due to the complexity of preparation process and inferior stability, it is still a great challenge to

develop simple and reliable strategies to produce genuinely stable photocatalysts. To date, novel Ag<sub>2</sub>Nb<sub>4</sub>O<sub>11</sub><sup>18</sup> and Ag<sub>2</sub>Ta<sub>4</sub>O<sub>11</sub> photocatalysts<sup>19</sup> have been reported. Both of them show the exceptional photocatalytic stability, but the disadvantage of them is that they can only response to the ultraviolet light due to the intrinsic large energy band gap (3.09 and 3.82 eV, respectively). Considering energy utilization and saving, it is particularly important to develop the highly efficient visible-light response Ag-based semiconductor photocatalysts with better stability.

Theoretically, the ligand-to-metal charge transfer (LMCT) which is related with resonance effect leads to decrease the energy of electronic transition, thus expanding light absorption range.<sup>20–22</sup> In addition, internal dipolar field is believed to aid carrier separation and transport, while the transformation between different intrinsic resonance structures can inhibit the reduction of Ag<sup>+</sup> ion.<sup>23</sup> According to reports, the molecular isocyanate NCO<sup>-</sup> ion commonly used as a reagent in organic and inorganic synthesis has been known for a long time.<sup>24</sup> And the resonance structures for the isocyanate ligand can be represented in three forms: N≡C–O<sup>-</sup> ↔ N=C=O ↔ N<sup>2-</sup>–C≡O<sup>+</sup>.<sup>25</sup> Based on those above reasons, if we adopt the new strategic method that the molecular isocyanate NCO<sup>-</sup> ion is combined with Ag<sup>+</sup> ion, the novel Ag-based photocatalysts may be equipped with superior photocatalytic stability under visible-light irradiation due to intrinsic resonance effect.

For the sake of realizing the above goal, in this work, we prepared a novel Ag-based photocatalyst, AgNCO, through a simple precipitation synthetic strategy. The as-prepared AgNCO sample not only responds to the wide visible-light region but also exhibits superior photocatalytic stability for degradation dyes. In addition, the positive influences of intrinsic resonance effect on light absorption, separation efficiency of charge carriers and stability of AgNCO are discussed in detail combined with calculation results based on density functional theory (DFT).

<sup>a</sup> Department of Chemistry, Harbin Institute of Technology, 150001, P. R. China, E-mail: gchen@hit.edu.cn, jxsun@hit.edu.cn.

<sup>b</sup> School of Materials Science and Engineering, Harbin Institute of Technology, 150001, P. R. China.

† Electronic Supplementary Information (ESI) available: [EDS and TEM]. See DOI: 10.1039/x0xx00000x

## Experimental

### Raw materials

The following chemicals were used: urea ( $\text{CH}_4\text{N}_2\text{O}$ ), silver nitrate ( $\text{AgNO}_3$ ), Titanium oxide ( $\text{TiO}_2$ ), Rhodamin B (RhB) and methylene blue (MB), benzoquinone ( $\text{C}_6\text{H}_4\text{O}_2$ ), ammonium oxalate ( $(\text{NH}_4)_2\text{C}_2\text{O}_4 \cdot \text{H}_2\text{O}$ ), dimethyl sulfoxide ( $(\text{CH}_3)_2\text{SO}$ ) were purchased from Aladdin Chemistry Co. Ltd. All reagents were of analytical grade and used as received without further purification. We used distilled water as the solvent.

### Synthesis of AgNCO sample

AgNCO can be synthesized by a simple precipitation process with  $\text{AgNO}_3$  solution. In a typical process, 6g (0.1mol) urea was first dissolved in 50 mL deionized water to form a clear solution. Then urea solution was transferred to a three-necked flask which was placed in an oil bath pot with a vigorous stirring for 6 hours at  $100^\circ\text{C}$ . 0.85g (0.005mol)  $\text{AgNO}_3$  was dissolved in 50mL deionized water, which was immersed into urea solution. After stirring for 10 min, the resulting grey suspension was transferred to the beaker and stirred for 20 minutes at room temperature to insure the reaction was completely. Subsequently, the system was kept static in the dark for 2 hours. The precipitations were washed in turn with secondary distilled water and absolute ethanol to dissolve any unreacted raw materials. Eventually, the obtained precipitate AgNCO products were dried at  $60^\circ\text{C}$ . For comparison, Nitrogen-doped  $\text{TiO}_2$  (N- $\text{TiO}_2$ ) was also synthesized according to a literature method.<sup>26</sup>

### Characterization of AgNCO sample

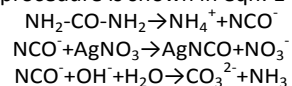
The phase of as-prepared AgNCO samples was characterized by powder X-ray diffraction (XRD, RigakuD/max-2000) equipped with a Philips PW3040/60 X-ray diffractometer at a scanning rate of  $5^\circ \text{min}^{-1}$  in the  $2\theta$  range of  $10\text{--}90^\circ$  using Cu K $\alpha$  radiation. X-ray tube current and voltage were set at 50 mA and 45 kV, respectively. Scanning electron microscopy (SEM) images were acquired using a scanning electron micro-analyzer with an accelerating voltage of 15 kV (FESEM, FEI QUANTA 200F). Energy dispersive X-ray spectrometry (EDS) was performed with a spectroscope attached to SEM, which was used for elemental analysis. Transmission electron microscope (TEM) of the samples was carried out on FEI TecnaiG2 S-Twin operating at 300 kV. Further evidence for the composition of the product was obtained from X-ray photoelectron spectroscopy (XPS) using an American electronics physical HI5700ESCA system with X-ray photoelectron spectroscope using Al K $\alpha$  (1486.6 eV) monochromatic X-ray radiation. Fourier transform infrared spectra were measured utilizing IR Affinity-1 FT-IR spectrometer. The absorption spectra of the as-prepared samples were measured at room temperature using a UV-vis spectrophotometer (PG, TU-1900) with  $\text{BaSO}_4$  as the background between 250 nm and 1200 nm at room temperature.

### Photocatalytic reaction

RhB and MB dyes were used to evaluate the photocatalytic activities of the as-obtained AgNCO sample. The degradation of RhB and MB dyes were performed in quartz photochemical reactor under visible-light illumination provided by a 300 W Xenon lamp (Trusttech PLS-SXE 300, Beijing) equipped with an ultraviolet cutoff filter and/or band pass filter to provide visible-light with  $\lambda \geq 400$  nm and/or monochromatic central wavelength visible-light with 550 nm and 420 nm ( $\lambda = \pm 15$  nm), respectively. All experiments were conducted at room temperature in air. In a typical process, RhB solution or MB solution ( $10 \text{ mg L}^{-1}$ , 100 mL) containing 0.1g AgNCO or 0.1g N- $\text{TiO}_2$  used for comparison was carried out. After being dispersed in an ultrasonic bath for 5 min, the mixture was stirred for 30 min in the dark to reach adsorption-desorption equilibrium between the catalyst and the solution under continuous magnetic stirring. Then, the suspension was exposed to visible-light irradiation. Every 30 min of time intervals, 3 mL mixture was collected from the suspension, and then they were centrifuged at 10000 rpm for 5 min to remove the photocatalysts. The concentrations of RhB or MB were measured the absorbance at  $\lambda = 554$  nm or  $\lambda = 664$  nm with the UV-vis spectrophotometer (PG, TU-1900).

## Results and discussion

Our design philosophy for the synthesis of AgNCO mainly utilizes the decomposition of urea at a higher temperature.<sup>27-28</sup> It is reported that urea solution refluxes for several hours can generate a large amount of  $\text{NCO}^-$  ions accompanied by a rise of pH value simultaneously. Then the supplementary  $\text{AgNO}_3$  solution acts as not only a donor of  $\text{Ag}^+$  ions but also a pH value regulator for the urea solution and avoids the transformation of  $\text{NCO}^-$  to  $\text{CO}_3^{2-}$ . The reaction mechanism of the preparation procedure is shown in eqn. 1



**Eqn. 1** Reaction mechanism for the decomposition of urea and the production of AgNCO.

The phase purity and crystallographic structure of the as-prepared AgNCO sample are investigated by XRD. As can be seen in the XRD patterns from Fig. 1, all the diffraction peaks

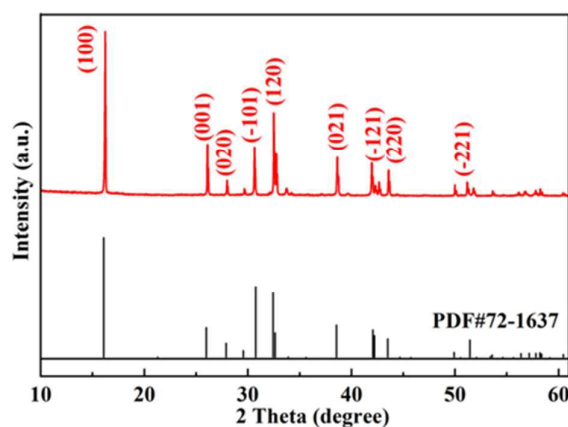


Fig. 1 XRD pattern of the as-prepared AgNCO sample.

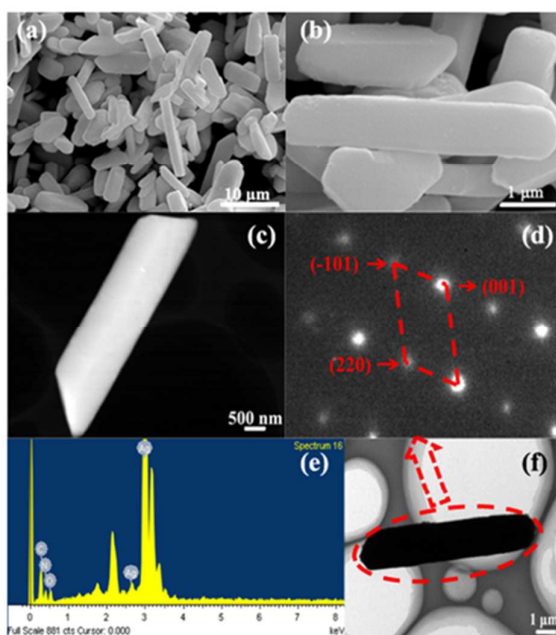


Fig. 2 SEM image (a, b), HAADF image (c), SAED pattern (d), EDS spectrum (e) and TEM image (f) of AgNCO sample.

can be indexed to monoclinic structure AgNCO (JCPDS#72-1637) satisfactorily, and no diffraction peaks from the impurities are detected. Moreover, the resulting sharp and intense diffraction peaks also indicate the AgNCO sample has high crystallinity. The results demonstrate that identical crystalline phase AgNCO sample is obtained.

In order to get the information of morphology and microstructure of AgNCO sample, the characterization of SEM and TEM is performed. The low magnified SEM image of AgNCO sample in Fig. 2a shows the obtained product is composed of rod-like particles. Meanwhile, the high magnified SEM image in Fig. 2b presents that the surface of AgNCO sample is smooth. Furthermore, the High Angle Annular Dark Field (HAADF) image shown in Fig. 2c further exhibits the smooth surface of AgNCO sample, which is consistent with the result of SEM image. The smooth surface of sample may be beneficial for charge carrier migration.<sup>29</sup> The HAADF image of a single AgNCO particle also shows the homogeneity of the elements about the whole particle due to a uniform distribution of light and dark.<sup>30-31</sup> Moreover, Selected Area Electron Diffraction (SAED) in Fig. 2d is performed on the whole particle (Fig. 2f), in which the diffraction pattern shows distinctly symmetrical diffraction spots, demonstrating that the AgNCO photocatalyst presents the characteristics of the single crystal.<sup>32</sup> In addition, the diffraction spots in the SAED pattern of the sample in Fig. 2d correspond to (-101) (001) and (220) crystal planes in monoclinic AgNCO crystal. The EDS spectrum of Fig. 2e presents that the sample is composed of Ag, N, C and O elements. It further certifies that the pure AgNCO sample is achieved.

Furthermore, the elemental composition and chemical state of the as-obtained AgNCO sample are investigated by XPS. The XPS survey spectra in Fig. S1 shows that the sample is composed of Ag, N, C and O elements, which is in accordance

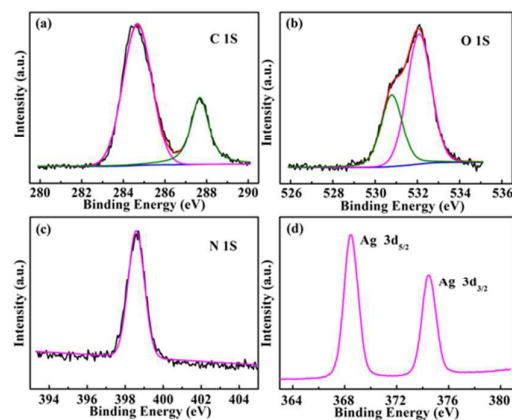


Fig. 3 High-resolution XPS spectra of the AgNCO sample C 1s (a), O 1s (b), N 1s (c) and Ag 3d (d).

with the results from EDS. The high-resolution XPS spectrum of C 1s displayed in Fig. 3a shows two peaks at 284.61 eV and 287.7 eV, which can be correspondingly ascribed to the lattice C 1s state of AgNCO and the carbon of hydrocarbon contaminants.<sup>29</sup> In addition, Fig. 3b shows the high-resolution XPS spectrum of O 1s, featured with two peaks at 530.8 and 532.1 eV, which is in line with the lattice O 1s state of AgNCO and adsorbed hydroxyl species, respectively.<sup>14</sup> The binding energy peak at 398.6 eV displayed in Fig. 3c is definitely the lattice N 1s state of AgNCO which can be assigned to  $sp^2$  hybridized N bonded to carbon atoms (C=N-).<sup>33</sup> It is found that the peaks of Ag 3d<sub>5/2</sub> and Ag 3d<sub>3/2</sub> are located at 368.4 eV and 374.4 eV in Fig. 3d. Due to the no-broadening and symmetric peak, it is believed that silver may only possess one Ag<sup>+</sup> chemical state and no other Ag nanoparticles generates,<sup>34</sup> which is in line with the HAADF image.

In addition, the existence and bonding mode of the NCO<sup>-</sup> anion in AgNCO are detected by FT-IR spectrum. As shown in Fig. 4, the absorption peaks at 1297  $cm^{-1}$  and 1207  $cm^{-1}$ , 636  $cm^{-1}$  are assigned to the pseudosymmetric stretching (C—O) and the bending (N≡C—O) vibration for NCO<sup>-</sup> ion.<sup>35-37</sup> There are two sharp peaks occurred at 2489  $cm^{-1}$  and 2395  $cm^{-1}$  respectively, which are assigned to the asymmetry stretching

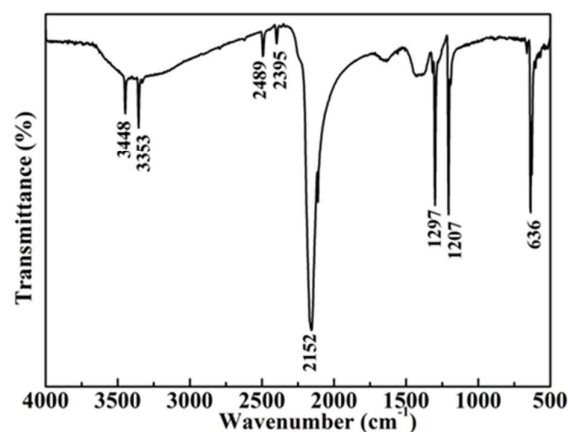


Fig. 4 The infrared spectrum of AgNCO sample.

## ARTICLE

vibration of cumulative double bond of (N=C=O).<sup>36</sup> It is noted that a strong absorption at 2152 cm<sup>-1</sup> matches the characteristic group frequencies of the antisymmetric stretching of C≡N.<sup>38-44</sup> However, the sp<sup>2</sup> hybridized N bonded to carbon atoms (C=N-) existed in NCO<sup>-</sup> is detected by XPS at the same time. The different types of chemical bonds between C and N atoms are perfectly consistent with the resonance structural formula of NCO<sup>-</sup>. Therefore it verifies the resonance effect existence of NCO<sup>-</sup> in AgNCO. The absorption peak at 3448 cm<sup>-1</sup> and 3353 cm<sup>-1</sup> can be assigned to adsorbed hydroxyl species, which is in consistent with XPS results. The absence of any absorption at 1500 cm<sup>-1</sup> in the IR spectrum suggests no presents of CO<sub>3</sub><sup>2-</sup> ion either as impurity phases,<sup>45</sup> which is in accord with the result of XRD. Combining the above results, it can be concluded that a novel photocatalyst AgNCO have been prepared successfully and the existence of intrinsic resonance effect in AgNCO is also solid confirmed.

The light absorption capacity of AgNCO sample is measured by the UV-Vis absorption spectrum. Fig. 5 exhibits that the absorption edge of AgNCO exists at around 530 nm. And the semiconductor band gap of AgNCO is estimated with empirical equations  $\alpha hv = A(hv - E_g)^n$ , where  $\alpha$ ,  $\nu$ ,  $A$ ,  $E_g$ , and  $n$  are the absorption coefficient, incident light frequency, constant, band gap, and an integer, respectively. And  $n$  decides the characteristics of the transition in a semiconductor. We define AgNCO belongs to indirect bandgap semiconductor and the value of  $n$  is calculated as 2, which is also demonstrated by theoretical calculation result below. Therefore, the bandgap of AgNCO is estimated to 2.6 eV shown in the insert of Fig. 5.<sup>46-47</sup> Meanwhile, VB and CB positions are calculated by means of using the empirical formula  $E_{VB} = X - E_e + 0.5E_g$  and  $E_{CB} = E_{VB} - E_g$ , where  $E_{VB}$ ,  $X$ ,  $E_e$ ,  $E_g$  and  $E_{CB}$  are the energy of the VB edge potential, the absolute electronegativity, free electrons on the hydrogen scale (4.5 eV), the band gap energy and the CB edge potential of the semiconductor, respectively. Therefore,  $E_{CB}$  and  $E_{VB}$  are estimated to be 0.52 eV and 3.12 eV, respectively. It's worth noting that there is a great absorption of visible-light of the sample in the wavelength range from 550 to 850 nm exhibited in Fig. 5, which can be attributed to the ligand-to-metal charge transfer (LMCT) absorptions of the AgNCO.<sup>20-22</sup> Simultaneously the ligand polarization existed in AgNCO which is caused by intrinsic resonance effect from the shift of electronic among  $N \equiv C - O^- \leftrightarrow N^- = C = O \leftrightarrow N^2- - C \equiv O^+$ . We

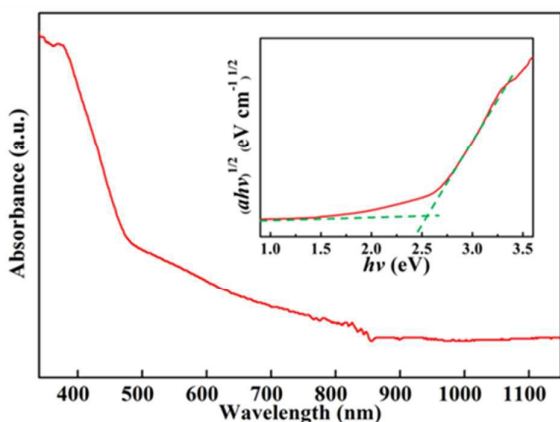


Fig. 5 UV-visible spectra and the plots of the  $(\alpha hv)^{1/2}$  versus photon energy (inset) of AgNCO sample.

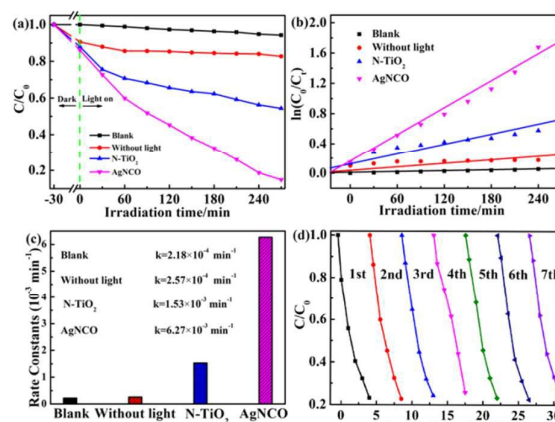


Fig. 6 Dynamic curves of photodegradation (a), plots of  $\ln(C_0/C)$  versus time (b) and rate constant  $k$  (c) for RhB solutions over AgNCO and N-TiO<sub>2</sub> samples under visible light, cycle runs of the photodegradation the RhB solution (d) over AgNCO sample.

surmise that the different intrinsic resonance structures of NCO<sup>-</sup> ligand will affect LMCT absorptions in turn due to a change of electrons density donated to the metal.<sup>48,49</sup> In conclusion, this LMCT actually affects the UV-visible absorption and thus AgNCO exhibits a significant enhancement in light absorption intensity in the whole visible light region.

The photocatalytic activity of AgNCO sample is investigated by the photocatalytic degradation experiments of the organic dye RhB in aqueous solutions under visible-light irradiation. The degradation kinetics curves of RhB solution (Fig. 6a) show that the photolysis is negligible without photocatalyst. And the concentration of RhB decreases relatively slowly in the dark compared to visible-light irradiation. Furthermore, AgNCO exhibits improved degradation efficiency compared with that of N-TiO<sub>2</sub>, which can almost completely remove RhB within 270 min. Moreover, from the UV-visible spectral changes of RhB in Fig. S2, the apparent decrease in absorption of RhB dye with a accompany wavelength shift of the band to shorter wavelengths confirms the dye is de-ethylated in a stepwise manner.<sup>50</sup> In view of that the pollutant is limited to the millimolar concentration range, the reaction kinetics of RhB photodegradation by the as-prepared photocatalysts can be described by pseudo first-order kinetics in terms of the Langmuir-Hinshelwood model<sup>51</sup> (eqn (2))  $\ln C_t = -kt + \ln C_0$  (2) where  $C_0$  is the initial dye concentration,  $C_t$  is the dye concentration in solution at time  $t$ , and  $k$  is the first-order rate constant. The kinetic plots of the AgNCO and TiO<sub>2</sub> are shown in Fig. 6b. The removal rate constant  $k$  of RhB photodegradation over AgNCO is  $6.27 \times 10^{-3} \text{ min}^{-1}$ , which reaches to 4.1, 24.4 and 28.7 times as much as that of N-TiO<sub>2</sub> ( $1.53 \times 10^{-3} \text{ min}^{-1}$ ), dark ( $2.57 \times 10^{-4} \text{ min}^{-1}$ ) and blank ( $2.18 \times 10^{-4} \text{ min}^{-1}$ ), respectively. In addition, we explore the dominant effect of the different kinds of activated species based on suppressive degree of degradation rate of them in photoreaction process. It indicates that the photodegradation over AgNCO photocatalyst mainly depends on the self-oxidation of semiconductor (shown in Fig. S5).<sup>52</sup>

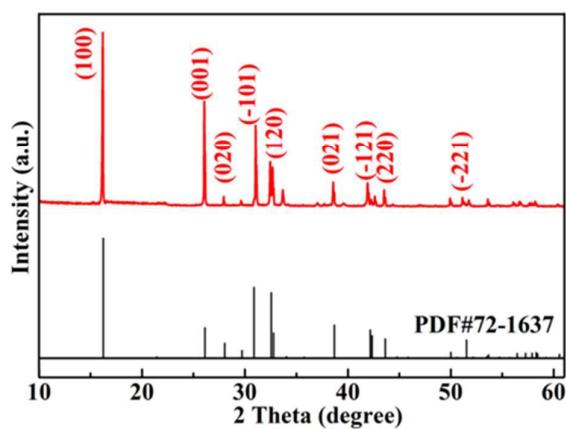


Fig. 7 XRD pattern of AgNCO sample after circle runs of RhB dye degradation.

The purpose of recycling experiments is to detect the stability and reusability of the samples. Take the practical application into consideration, the photocorrosion of Ag-based photocatalyst are highlighted. Therefore, it is particularly important for Ag-based photocatalyst with an exceptional photocatalytic stability. Herein, the stability of photocatalysts for the degradation of RhB is chosen. The result is shown in Fig. 6d, it seems to be only a little loss of the photocatalytic activity over AgNCO sample after the 7 cycles about 30 hours, which verifies the as-prepared AgNCO sample has unique photocatalytic stability under visible light. Besides, the XRD pattern of AgNCO sample after 7 cycles is nearly unchanged compared with the fresh sample (Fig. 7) and no Ag phase is detected, which also indicates that AgNCO is a relatively stable Ag-based photocatalyst. What's more, even when MB dye serves as target molecules, the removal rate is also higher than that of N-TiO<sub>2</sub> shown in Fig. S3a. It can almost entirely remove MB within 240 min. The rate constant of the photodegradation of MB over AgNCO is  $8.41 \times 10^{-3} \text{ min}^{-1}$  displayed in Fig. S3c, which reaches to 3.28, 16.8 and 25.4 times as much as that of N-TiO<sub>2</sub> ( $2.56 \times 10^{-3} \text{ min}^{-1}$ ), dark ( $5.01 \times 10^{-4} \text{ min}^{-1}$ ) and blank ( $3.31 \times 10^{-4} \text{ min}^{-1}$ ), respectively. Note that there is almost no shift of absorption peak located at 667 nm shown in Fig. S3d, indicating that the benzene/heterocyclic rings of MB molecule are decomposed into small organic/inorganic molecules or ion products.<sup>53</sup> The above results indicate that AgNCO photocatalyst exhibits universality for the degradation of various organic dyes, enhanced photocatalytic degradation ability and excellent photocatalytic stability.

The possible photocatalytic reaction mechanism and the carrier separation behavior promoted by intrinsic resonance effect over the AgNCO sample are shown in Fig. 8. Considering that the atomic partial charges are not symmetrically distributed in the isocyanate anion,<sup>54</sup> intrinsic resonance effect in conjunction with internal dipolar fields is believed to aid carrier separation and transport. Meanwhile, the band gap of AgNCO is 2.4 eV and thus can be excited under visible-light radiation. The charge carrier separation and transfer behavior suffered from a cycle shown in Fig. 8. Firstly, the electron from valence-band maximum (VBM) composed of Ag 5d, N 2p and O 2p excited into conduction-band minimum (CBM) composed of

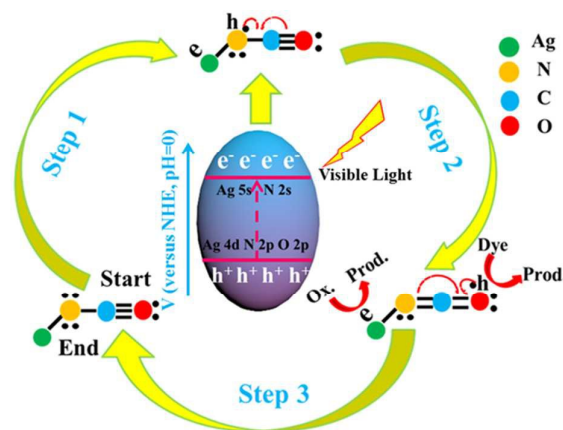


Fig. 8 The possible photocatalytic reaction mechanism and the carrier separation behavior over AgNCO sample.

Ag 5s and N 2s,<sup>23</sup> resulting in electron-hole pair formation. (Step1) Then, due to the intrinsic resonance effect of AgNCO and strong electronegativity of O, internal dipolar field generate and it can promote the separation of electron and hole. Electron transfers from Ag on the left and one p bond of O≡C breaks to convert the N<sup>2-</sup>-C≡O<sup>+</sup> group to N<sup>-</sup>=C=O group. (Step2) Subsequently, the electron will react with oxygen to generate superoxide radicals ( $\bullet\text{O}_2^-$ ). The  $\bullet\text{O}_2^-$  active species and  $\bullet\text{OH}$  radicals are responsible for the degradation of RhB and MB, respectively (shown in Fig. S4). Ultimately, N<sup>-</sup>=C=O group gets back to the initial N<sup>2-</sup>-C≡O<sup>+</sup> state, a cycle finishes under visible light (Step3) and goes on continuously. Once electrons and holes have migrated away from their production sites, these above processes may accelerate electrons and holes to participate in the reaction with oxygen and dyes in time. The transformation between different intrinsic resonance structures reduces the reaction opportunity of electronics and Ag<sup>+</sup> ion. In consequence, the intrinsic resonance effect suppresses the reduction of Ag<sup>+</sup> ion and increases the photocatalytic stability of AgNCO effectively.

Furthermore, in order to confirm the position of the electrons and holes of AgNCO photocatalyst, we calculated the band structure and the density of states (DOS) for Ag, C, O and N near the Fermi level (EF) using first-principles DFT shown in Fig. 9 (see calculation method of theory, Supporting Information). The corrected bandgap dispersion of AgNCO in Fig. 9a proves that AgNCO belongs to an indirect bandgap semiconductor according with the result shown in the absorption spectrum.<sup>55</sup> The calculated partial DOS suggests that the valence band is mainly composed of Ag 4d orbitals hybridized with N 2p, N 2s, O 2s, O 2p, C 2s and C 2p orbitals, and the conduction band primarily consists of Ag 5s, Ag 5p, N

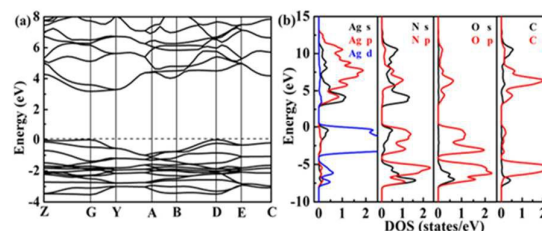


Fig. 9 Band structure (a) and partial DOS (b) of AgNCO sample.

## ARTICLE

## Journal Name

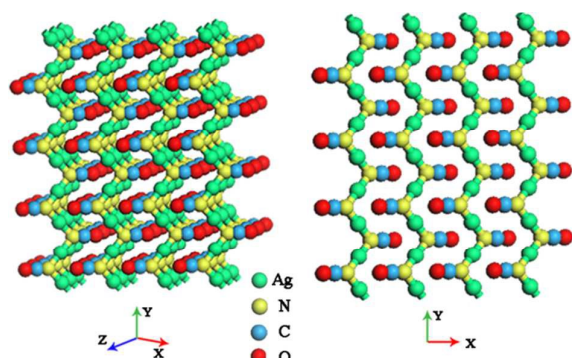


Fig. 10 Crystal structure schematic of AgNCO sample.

2p, N 2s, C 2p and O 2p orbitals. More specifically, it indicates that the VB of AgNCO is dominated by Ag 4d, N 2p, O 2p and the CB consists of Ag 5s, N 2s, which proves the accuracy of the proposed photocatalytic reaction mechanism above.<sup>56</sup> At the same time, the hybridization of orbitals favors high electron mobility, which may avoid the reduction of Ag<sup>+</sup> ion.

The crystal structure of AgNCO is another important factor to be equipped with the exceptional photocatalytic stability, according to reports.<sup>57</sup> As is shown in Fig. 10, The AgNCO compound is composed of zigzag chains along the Y-axis in which the silver cation is in a two-fold coordination of  $-(O_2C_2N_2)Ag(N_2C_2O_2)^-$ .<sup>25</sup> The  $NCO^{-1}$  acts as a bridge to contact the Ag atoms on both ends of the bond, leading to a 180° angle of N-Ag-N formation which is in favor of the migration of electrons and holes.<sup>16</sup> Meanwhile, on account of high electron mobility, the strong electronegativity of the terminal N of N-Ag-N bond and the transformation between different intrinsic resonance structures may inhibit the nonlocalized electrons to react with Ag<sup>+</sup> ions and thus prevent Ag<sup>+</sup> ion from reduction. As mentioned above, this compound contains zig-zag Ag-N-Ag chains with a bond angle of 95.847°, which prevents the overlap of electron cloud of adjacent atoms of Ag-Ag to protect Ag<sup>+</sup> from reducing.<sup>24</sup> Additionally, the layered structure of AgNCO may facilitate the transport and separation of the carrier.<sup>58</sup> All the above features are beneficial to strengthen the photocatalytic stability of AgNCO for the degradation of RhB and MB dyes.

## Conclusions

In summary, we have successfully synthesized a novel visible-light sensitive Ag-based photocatalyst AgNCO by a simple precipitation reaction. The as-prepared AgNCO exhibits enhanced photocatalytic activity and excellent photocatalytic stability for the degradation of RhB and MB under visible-light irradiation. The superior photocatalytic stability may be attributed to the intrinsic resonance effect and crystal structure of AgNCO. Meanwhile, the intrinsic resonance effect can promote the separation and migration of photogenerated electrons and holes, thus improving the photocatalytic activity. This work develops a novel photostabilized Ag-based photocatalyst employing the intrinsic resonance effect under visible-light irradiation, which may play a guidance role in Ag-based photocatalysts development.

## Acknowledgements

This work was financially supported by projects of Natural Science Foundation of China (21271055 and 21471040), the Fundamental Research Funds for the Central Universities (HIT-IBRSEM. A. 201410). We acknowledge for the support by Open Project of State Key Laboratory of Urban Water Resource and Environment, Harbin Institute of Technology (No.QAK201304) and Program for Innovation Research of Science in Harbin Institute of Technology (PIRS of HIT B201412).

## Notes and references

- S. Q. Liu, Z. R. Tang, Y. G. Sun, J. C. Colmenares and Y. J. Xu, *Chem. Soc. Rev.*, 2015, 44, 5053-5075.
- K. Maeda, K. Teramura, D. L. Lu, N. Saito, Y. Inoue and K. Domen, *Angew. Chem., Int. Ed.*, 2006, 45, 7806-7809.
- C. M. Li, G. Chen, J. X. Sun, Y. J. Feng, J. J. Liu and H. J. Dong, *Appl. Catal., B*, 2015, 163, 415-423.
- J. J. Li, Y. L. Xie, Y. J. Zhong and Y. Hu, *J. Mater. Chem. A*, 2015, 3, 5474-5481.
- Y. P. Bi, S. X. Ouyang, N. Umezawa, J. Y. Cao, and J. H. Ye, *J. Am. Chem. Soc.*, 2011, 133, 6490-6492.
- L. Ni, M. Tanabe and H. Irie, *Chem. Commun.*, 2013, 49, 10094-10096.
- K. Maeda, A. K. Xiong, T. Yoshinaga, T. Ikeda, N. Sakamoto, T. Hisatomi, M. Takashima, D. L. Lu, M. Kanehara, T. Setoyama, T. Teranishi, and K. Domen, *Angew. Chem.*, 2010, 122, 4190-4193.
- S. X. Ouyang and J. H. Ye, *J. Am. Chem. Soc.*, 2011, 133, 7757-7763.
- H. F. Shi, Z. S. Li, J. H. Kou, J. H. Ye and Z. G. Zou, *J. Phys. Chem. C*, 2011, 115, 145-151.
- J. Boltersdorf, T. Wong and P. A. Muggard, *ACS Catal.*, 2013, 3, 2943-2953.
- M. Li, J. Zhang, W. Dang, S. K. Cushing, D. Guo, N. Wu and P. Yin, *Phys. Chem. Chem. Phys.*, 2013, 15, 16220-16226.
- T. Y. Huang, Y. J. Chen, C. Y. Lai and Y. W. Lin, *RSC Adv.*, 2015, 5, 43854-43962.
- P. H. Wang, Y. X. Tang, Z. L. Dong, Z. Chen and T. Lim, *J. Mater. Chem. A*, 2013, 1, 4718-4727.
- N. Zhang, M. Q. Yang, S. Q. Liu, Y. G. Sun, and Y. J. Xu, *Chem. Rev.*, 2015, 115, 10307-10377.
- L. Yuan, Y. J. Xu, *Appl. Surf. Sci.*, 2015, 342, 154-167.
- S. W. Zhang, J. X. Li, X. K. Wang, Y. S. Huang, M. Y. Zeng and J. Z. Xu, *J. Mater. Chem. A*, 2015, 3, 10119-10126.
- H. Tong, S. X. Ouyang, Y. P. Bi, N. Umezawa, M. Oshikiri and J. H. Ye, *Adv. Mater.*, 2012, 24, 229-251.
- H. J. Dong, G. Chen, J. X. Sun, Y. J. Feng, C. M. Li and C. D. Lv, *Chem. Commun.*, 2014, 50, 6596-6599.
- H. J. Dong, J. X. Sun, G. Chen, C. M. Li, Y. D. Hu and C. D. Lv, *Phys. Chem. Chem. Phys.*, 2014, 16, 23915-23921.
- C. C. Chen, W. H. Ma and J. C. Zhao, *Chem. Soc. Rev.*, 2010, 39, 4206-4219.
- G. Zhang, G. Kim and W. Y. Choi, *Energy Environ. Sci.*, 2014, 7, 954-966.
- Y. K. Shin, B. S. Brunshwig, C. Creutz, and N. Sutin, *J. Am. Chem. Soc.*, 1995, 117, 8668-8669.
- W. Zhao, Y. F. Liu, J. J. Liu, P. Chen, W. Chen, F. Q. Huang and J. H. Lin, *J. Mater. Chem. A*, 2013, 1, 7942-7948.
- J. Nelson and S. M. Nelson, *J. Chem. Soc.*, 1969, 1597-1603.
- D. J. Williams, S. C. Vogel and L. L. Daemen, *Phys. B*, 2006, 385, 228-230.
- Z. G. Yi, J. H. Ye, N. Kikugawa, T. Kako, S. X. Ouyang, H. Stuart-Williams, H. Yang, J. Y. Cao, W. J. Luo, Z. S. Li, Y. Liu, R. L. Withers, *Nat. Mater.*, 2010, 9, 559-564.

- 27 M. Angeles Larrubi, G. Ramis and G. Busc, *Appl. Catal., B*, 2000, **27**, 145-151.
- 28 A. Alahmad, M. Eleoui, A. Falah and I. Alghoraibi, *Physical Sciences Research International*, 2013, **1**, 89-96.
- 29 H. J. Dong, G. Chen, J. X. Sun, C. M. Li, Y. G. Yu and D. H. Chen, *Appl. Catal., B*, 2013, **134**, 46-54.
- 30 M. Porcu, A. K. Petford-Long and J. M. Sykes, *J. Alloy. Compd*, 2008, **453**, 341-346.
- 31 M. K. Devaraju, Q. D. Truong and I. Honma, *RSC Adv.*, 2013, **3**, 20633–20638.
- 32 J. S. Jie, W. J. Zhang, Y. Jiang, X. M. Meng, Y. Q. Li, and S. T. Lee, *Nano Lett*, 2006, **6**, 1887-1892.
- 33 Y. P. Liu, L. Fang, H. D. Lu, Y. W. Li, C. Z. Hu and H. G. Yu, *Appl. Catal., B*, 2012, **115**, 245-252.
- 34 Z. H. Chen, F. Bing, Q. Liu, Z. G. Zhang and X. M. Fang, *J. Mater. Chem. A*, 2015, **3**, 4652-4657.
- 35 A. Popitsch, E. Nachbaur and H. P. Fritzer, *J. Mol. Struct.*, 1986, **143**, 41-46.
- 36 A. Maki and J. C. Decius, *J. Chem. Phys.*, 1958, **28**, 1003-1004.
- 37 J. Martínez-Lillo, D. Armentano, G. D. Munno, F. Lloret, M. Julve and J. Faus, *Inorg. Chim. Acta*, 2006, **359**, 4343-4345.
- 38 B. Mavis and M. Akinc, *Chem. Mater.*, 2006, **18**, 5317-5325.
- 39 N. J. Nelson, N. E. Kime and D. F. Shriver, *J. Am. Chem. Soc.*, 1969, **91**, 5173-5275.
- 40 B. Mavis, and M. Akinc, *J. Am. Ceram. Soc.*, 2006, **89**, 471-477.
- 41 D. Nicola, C. Effendy, Fazaroh, F. Pettinari, C. Skelton, B. W. Somers, N. and White, A. H. *Inorg. Chim. Acta*, 2005, **358**, 720-734.
- 42 P. Rabu, S. Angelov, P. Legoll, M. Belaiche and M. Drillon. *Inorg. Chem.*, 1993, **32**, 75-78.
- 43 T.N. Ramesh and P. Vishnu Kamath, *J. Power. Sources*, 2006, **156**, 655-661.
- 44 C. L. Schmidt and M. Jansen, *J. Mater. Chem.*, 2010, **20**, 110-116.
- 45 Y. Du and D.O'Hare, *Inorg. Chem.*, 2008, **47**, 3234-3242.
- 46 J. X. Sun, G. Chen, Y. X. Li, R. C. Jin, Q. Wang and J. Pei, *Energy Environ. Sci.*, 2011, **4**, 4052-4060.
- 47 S. Bai, J. Jiang, Q. Zhang and Y. J. Xiong, *Chem. Soc. Rev.*, 2015, **44**, 2893-2939.
- 48 K. M. Milum, Y. N. Kim, and Bradley J. Holliday, *Chem. Mater.*, 2010, **22**, 2414-2416.
- 49 C. V. Sastri, M. J. Park, T. Ohta, T. A. Jackson, A. Stubna, M. S. Seo, J. Lee, J. Kim, T. Kitagawa, E. Münck, L. Q., Jr., and W. Nam, *J. Am. Chem. Soc.*, 2005, **127**, 12494-12495.
- 50 L. Ge, C. C. Han and J. Liu, *Appl. Catal., B*, 2011, **108**, 100-106.
- 51 X. F. Hu, T. Mohamood, W. H. Ma, C. C. Chen and J. C. Zhao, *J. Phys. Chem. B*, 2006, **110**, 26012-26015.
- 52 L. Yuan, M. Q. Yang and Y. J. Xu, *Nanoscale*, 2014, **6**, 6335-6345.
- 53 C.H. An, S. Peng, and Y. G. Sun, *Adv. Mater.*, 2010, **22**, 2570-2575.
- 54 C. L. Schmidt, R. E. Dinnebier and M. Jansen, *Solid. State. Sci.*, 2009, **11**, 1107-1113.
- 55 J. G. Yu, Q. J. Xiang and M. H. Zhou, *Appl. Catal., B*, 2009, **90**, 595-602.
- 56 P. Zhou, J. G. Yu and Y. X. Wang, *Appl. Catal., B*, 2013, **142**, 45-53.
- 57 G. Q. Tan, L. L. Zhang, H. J. Ren, S. S. Wei, J. Huang and A. Xia, *ACS Appl. Mater. Interfaces*, 2013, **5**, 5186–5193.
- 58 M. L. Guan, C. Xiao, J. Zhang, S. J. Fan, R. An, Q. M. Cheng, J. F. Xie, M. Zhou, B. J. Ye, and Y. Xie, *J. Am. Chem. Soc.*, 2013, **135**, 10411-10417.